AIP | Journal of Applied Physics

# Electrical transport and optical model of GaAs-AlInP core-shell nanowires

A. C. E. Chia, M. Tirado, Y. Li, S. Zhao, Z. Mi et al.

Citation: J. Appl. Phys. **111**, 094319 (2012); doi: 10.1063/1.4716011
View online: http://dx.doi.org/10.1063/1.4716011
View Table of Contents: http://jap.aip.org/resource/1/JAPIAU/v111/i9
Published by the American Institute of Physics.

# Electrical transport and optical model of GaAs-AlInP core-shell nanowires

A. C. E. Chia,[1] M. Tirado,[2] Y. Li,[3] S. Zhao,[3] Z. Mi,[3] D. Comedi,[4,5] and R. R. LaPierre[1,a)]
[1]*Department of Engineering Physics, Centre for Emerging Device Technologies, McMaster University, Hamilton, Ontario L8S 4L7, Canada*
[2]*Laboratorio de Propiedades Dieléctricas de la Materia, Dep. de Física, FACET, Universidad Nacional de Tucumán, Avenida Independencia 1800, 4000 Tucumán, Argentina*
[3]*Department of Electrical and Computer Engineering, McGill University, Montreal, Quebec H3A 2A7, Canada*
[4]*Laboratorio de Física del Sólido, Dep. de Física, FACET, Universidad Nacional de Tucumán, Avenida Independencia 1800, 4000 Tucumán, Argentina*
[5]*Consejo Nacional de Investigaciones Científicas y Técnicas (CONICET), Buenos Aires Argentina*

(Received 19 March 2012; accepted 23 March 2012; published online 15 May 2012)

GaAs nanowires were passivated by AlInP shells grown by the Au-assisted vapor-liquid-solid method in a gas source molecular beam epitaxy system. Transmission electron microscopy confirmed a core-shell GaAs-AlInP structure. Current-voltage measurements on ensemble nanowires indicated improved carrier transport properties in the passivated nanowires as compared to their unpassivated counterpart. Similarly, individual nanowires showed improved photoluminescence intensity upon passivation. A detailed model is presented to quantify the observed improvements in nanowire conduction and luminescence in terms of a reduction in surface charge trap density and surface recombination velocity upon passivation. The model includes the effects of high-level injection, bulk recombination, and surface recombination. The model can be used as a tool for assessing various passivation methods. © *2012 American Institute of Physics*.
[http://dx.doi.org/10.1063/1.4716011]

## INTRODUCTION

Semiconductor nanowires have diverse applications in next generation photovoltaic, light emitting diode, sensor, photodetector, and transistor devices.[1] Nanowires are one-dimensional rods with a diameter typically on the order of 10 to 100 nm and a length (typically a few microns) that is much greater than their diameter. Nanowires are most commonly fabricated using the vapor-liquid-solid (VLS) method in which a metal nanoparticle (usually Au) is used as a seed particle to collect vapor-deposited material during molecular beam epitaxy (MBE) or metalorganic vapor phase epitaxy (MOVPE).[2] Nanowire heterostructures can be fabricated by switching the material during growth. Thus, axial heterostuctures (along the nanowire length) or radial heterostructures (core-shell or coaxial structures) can be fabricated for optoelectronic device applications.

Core-shell heterostructures enable the passivation of nanowire surface/defect states to improve optical and electrical performance. The surfaces of most III-V semiconductors contain a high density of surface states causing Fermi level pinning near the middle of the bandgap. Fermi level pinning detrimentally affects the performance of semiconductor devices by creating Schottky barrier contacts and decreasing photogenerated carrier collection by increasing the surface recombination and surface depletion of carriers.[3] In nanostructures such as nanoparticles or nanowires, the effect of Fermi level pinning can be more pronounced due to the inherently large surface to volume ratio.

Surface passivation can be applied to reduce the detrimental effects of surface states. Charge carriers can be confined to the core of the nanowire and away from the surface by encapsulating the core in a larger bandgap shell (core-shell structure). Thus, depletion due to surface states and surface recombination of charge carriers along the nanowire sidewalls can be reduced. For example, AlGaAs shells have been recently shown to improve the photoluminescence (PL) from GaAs nanowires.[4] Similarly, time-resolved terahertz spectroscopy has shown a reduction in surface trap density of GaAs upon passivation by AlGaAs encapsulation.[5]

In the present contribution, the passivation of GaAs nanowires is presented using an $Al_xIn_{1-x}P$ shell instead of the more commonly used AlGaAs shell. When the Al fraction is near 0.52, $Al_xIn_{1-x}P$ is lattice-matched to GaAs. $Al_{0.52}In_{0.48}P$ has a large bandgap (2.47 eV at room temperature) and a small refractive index,[6] which makes it interesting for several optoelectronic applications. For example, AlInP is used as a "window layer" in the passivation of multi-junction solar cells,[7] and as the cladding layers in lasers, light emitting diodes, and modulators.[8] In this paper, we use current-voltage characteristics of ensemble nanowire devices, combined with photoluminescence, as a means of estimating the nanowire surface parameters [surface trap density and surface recombination velocity (SRV)]. We demonstrate that an AlInP shell can provide effective passivation for a GaAs nanowire core.

## EXPERIMENTAL DETAILS

GaAs nanowires were grown by the Au-assisted VLS method in a gas source MBE (GSMBE) system. Zn-doped n-type GaAs (111)B ($1–5 \times 10^{18}$ $cm^{-3}$) wafers were treated by UV-ozone oxidation for 20 min to remove any hydrocarbon contamination and to grow a sacrificial oxide. The

a)E-mail: lapierr@mcmaster.ca.

 

wafers were then dipped in buffered hydrofluoric (HF) acid for 30 s and rinsed under flowing deionized water for 10 min. The wafers were dried with $N_2$ and transferred to an electron beam evaporator where a 1 nm thick Au film was deposited at room temperature at a rate of 0.1 nm/s as measured by a quartz crystal thickness monitor. The wafers were then transferred to the GSMBE system (SVT Associates). In GSMBE, group III species (In, Ga, Al) are supplied as monomers from an effusion cell, and group V species (P, As) are supplied as $P_2$ and $As_2$ dimers that are cracked from $PH_3$ and $AsH_3$ in a gas cracker operating at 950 °C. Prior to growth, the wafers were placed in a pre-deposition chamber where they were degassed for 15 min at 300 °C. After transferring the wafers to the growth chamber, an oxide desorption step was performed where they were heated to 540 °C under inductively coupled hydrogen plasma and $As_2$ overpressure for 10 min, leading to the formation of Au nanoparticles.

The samples were heated to the growth temperature of 600 °C and GaAs nanowire growth was initiated by opening the Ga shutter. GaAs was grown for 30 min at a V/III flux ratio of 2.3 and an equivalent 2D growth rate of 0.14 nm/s. The nanowires were doped n-type with Te at a nominal level of $10^{18}$ $cm^{-3}$. The growth was then switched to $Al_{0.52}In_{0.48}P$, which is lattice-matched to GaAs. Growth conditions of the AlInP consisted of a substrate temperature of 500 °C, V/III flux ratio of 3.5, duration of 30 min, and 2D equivalent growth rate of 0.14 nm/s. The AlInP shells were nominally undoped. As will be presented below, these growth conditions resulted in a shell of AlInP surrounding the previously grown GaAs nanowire core. Two samples were grown: one with the AlInP shell and one without (i.e., with and without passivation of the GaAs nanowire surface).

After growth, the nanowire morphology was determined using a JEOL 7000F field emission scanning electron microscope (SEM). A representative SEM image of the as-grown GaAs-AlInP nanowires is shown in Figure 1. Based on the SEM analysis, the nanowires were roughly 2-3 $\mu$m in length. The average diameter of the unpassivated GaAs nanowires without the AlInP shell was 52 nm, while the diameter of the GaAs-AlInP nanowires was 95 nm, indicating an AlInP shell thickness of about 20 nm.

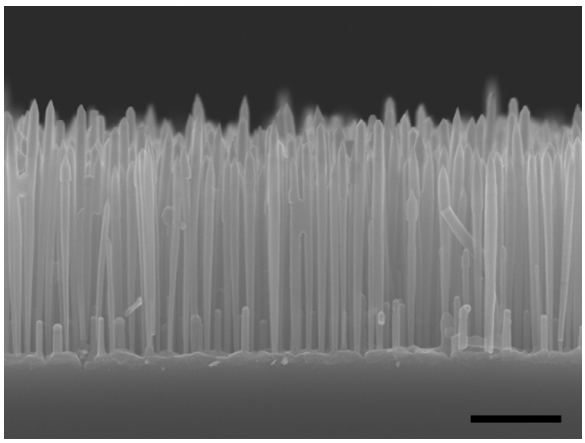

FIG. 1. Cross-sectional SEM image of GaAs-AlInP core-shell nanowires. Scale bar is 1 $\mu$m.

The nanowires were removed from the growth substrate by sonication in methanol solution followed by drop casting onto a holey carbon grid for structural analysis by a JEOL 2010F high resolution scanning transmission electron microscope (HRTEM). High angle annular dark field (HAADF) imaging was used where larger atomic mass appears as brighter contrast. The chemical composition was determined by energy dispersive x-ray spectroscopy (EDS) in the HRTEM. Figure 2 shows a representative HAADF image for a cross-sectional disc removed by a microtoming process from the GaAs-AlInP nanowire array. The bright contrast near the centre of the disc indicates the GaAs nanowire core as confirmed by the superimposed EDS linescans showing high counts of elemental Ga and As but negligible amounts of other elements in the core. The darker contrast near the edge of the nanowire indicates an AlInP shell, also confirmed by the EDS linescan showing Al, In, and P counts but negligible Ga and As counts. Hence, under the growth conditions employed, a GaAs core with an AlInP shell was produced. The thickness of the shell ascertained by TEM was ~20 nm, consistent with the SEM measurements described earlier.

Electrical studies were performed by deposition of Ni/Ge/Au contacts onto the ensemble as-grown nanowires using a procedure described previously.[9] In addition to the AlInP shell depicted in Figure 2, there is also some growth of AlInP axially on top of the passivated GaAs core. Therefore, the GaAs core is completely encapsulated in AlInP. I-V measurements (not shown) obtained on samples without removal of the AlInP shell from the top of the nanowires before contacting revealed negligible current, confirming that the undoped shell exhibited negligible conduction. Therefore, the highly resistive AlInP shell must be removed from the top portion of the nanowires to permit contacting to the GaAs core directly, while leaving the AlInP passivation

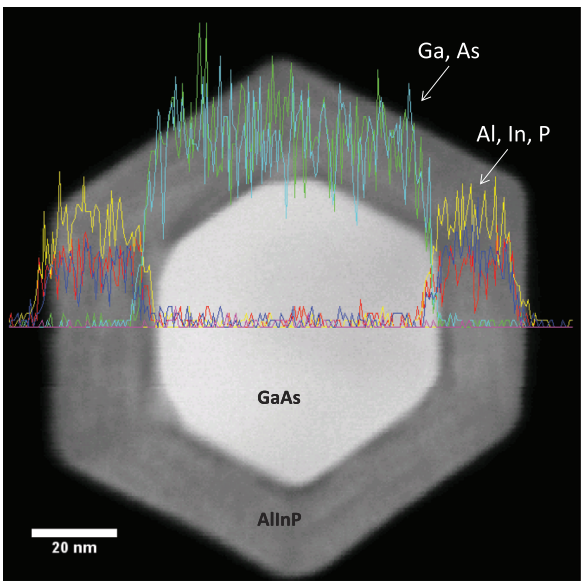


FIG. 2. HAADF image of microtomed cross-section of GaAs-AlInP core-shell nanowire showing GaAs core (bright contrast) and AlInP shell (dark contrast). Superimposed EDS linescans indicate the presence of Ga (green) and As (light blue) coinciding with the bright core, and Al (red), In (dark blue), and P (yellow) coinciding with the darker shell, confirming the GaAs-AlInP core-shell structure. Scale bar is 20 nm.

intact on the sidewalls of the nanowires. To expose the GaAs core for contacting, the nanowire surface was first planarized by spin-casting cyclotene polymer followed by reactive ion etching with oxygen plasma, leaving a polymer thickness of 1 $\mu$m. The tops of the nanowires exposed above the polymer layer were then removed by a sonication procedure such that all contacted nanowires were the same length (1 $\mu$m). The latter procedure removed the axial segment of the AlInP cladding above the GaAs core and exposed the GaAs core for contacting. The resulting current-voltage measurements are discussed in the Results section.

Room temperature PL was measured from nanowires that were dispersed randomly onto a silicon substrate covered by thermally grown 300 nm thick silicon dioxide. A semiconductor laser diode ($\lambda \sim 635$ nm) was used as the excitation source and the PL emission was analyzed using a high-resolution spectrometer and a single channel InGaAs photodiode with lock-in amplification. The resulting PL measurements are discussed in the Results section.

## MODEL DETAILS

Simulation of the nanowire current density versus voltage (J-V) characteristics was performed using COMSOL Multiphysics finite element analysis code to solve the continuity and Poisson equation in a single nanowire. The nanowire was treated as a cylindrical rod with length of 1 $\mu$m as obtained in the fabricated devices. The diameter of the GaAs core was set equal to a diameter of 52 nm. For the passivated nanowires, the AlInP shell thickness was set to 20 nm. The latter measurements were based on the SEM and TEM measurements of the unpassivated and passivated nanowires as described earlier. The doping of the GaAs core was assumed equal to the nominal n-type doping level of $N_d = 10^{18}$ cm$^{-3}$. The AlInP shell was assumed to be unintentionally doped n-type to $10^{16}$ cm$^{-3}$, although any shell doping level much less than that of the core ($10^{18}$ cm$^{-3}$) was found to have negligible effect on the simulated J-V characteristics. The nanowire model included a substrate (n-type doping level of $5 \times 10^{18}$ cm$^{-3}$) with lateral extent (radius) of 167 nm, corresponding to the average spacing between nanowires as assessed by plan view SEM images. Doping dependent carrier mobilities were used.[10]

The continuity and Poisson equation were solved in the nanowire using the Slotboom formalism as described in our previous work.[11] The Slotboom functions express the electron ($n$) and hole ($p$) densities as

$$n = n_i e^{q\psi/kT} u, \tag{1}$$

$$p = n_i e^{-q\psi/kT} v, \tag{2}$$

where $n_i$ is the intrinsic carrier concentration ($1.5 \times 10^6$ cm$^{-3}$ for GaAs), $\psi$ is the electric potential, and $u$ and $v$ are the Slotboom variables related to the quasi-Fermi levels of the carriers.

To include the effects of surface band bending (depletion) at the sidewall surfaces of the nanowire and the substrate surface surrounding the base of the nanowire, the surface boundary was treated with a surface charge. The boundary condition of the electric potential is[11,12]

$$\hat{n} \cdot \varepsilon_s \nabla\psi = q(D_d^+ - D_a^-), \tag{3}$$

where $\varepsilon_s$ is the permittivity of the semiconductor, $\hat{n}$ is the unit vector normal to the surface, and $D_d^+$ and $D_a^-$ are the surface densities (cm$^{-2}$) of ionized donor-type and acceptor-type traps, respectively, where[11,12]

$$D_d^+ = \frac{n_{dtrap} + n_i v e^{-q\psi/kT}}{n_i u e^{q\psi/kT} + n_{dtrap} + n_i v e^{-q\psi/kT} + p_{dtrap}} D_d \tag{4}$$

and

$$D_a^- = \frac{p_{atrap} + n_i u e^{q\psi/kT}}{n_i u e^{q\psi/kT} + n_{atrap} + n_i v e^{-q\psi/kT} + p_{atrap}} D_a, \tag{5}$$

$D_d$ and $D_a$ (assumed to be equal) are the density of the defect donor- and acceptor-type traps, respectively. $n_{dtrap}$ ($p_{dtrap}$) is the electron (hole) density in the conduction (valence) band if the Fermi level was located at the position of the donor-type surface trap which we assume is at the intrinsic energy level near midgap. $p_{atrap}$ and $n_{atrap}$ have similar meanings for the acceptor-type traps. A range of values of $D = D_d = D_a = 10^{12}$-$10^{13}$ cm$^{-2}$ was examined for unpassivated GaAs in accordance with Ref. 13. Similarly, for the passivated nanowires, a range of values $D$ was used for the trap density at the GaAs-AlInP interface. $D = 10^{13}$ cm$^{-2}$ was assumed for the AlInP free surface although this had a negligible effect on the model results due to the relatively large separation of this charge from the core by the shell thickness (20 nm).

The recombination rate of electrons and holes, which is important in the space-charge region of a nanowire, was treated using Shockley-Read-Hall (SRH) recombination in the Slotboom formalism

$$R_{SRH} = \frac{n_i(uv - 1)}{\tau_p(ue^{q\psi/kT} + 1) + \tau_n(ve^{-q\psi/kT} + 1)}, \tag{6}$$

where $\tau_n$ and $\tau_p$ are the electron and hole lifetimes, respectively, taken to be equal ($\tau = \tau_n = \tau_p$). The effect of bulk recombination on the model J-V curves was determined by varying $\tau$ from 1 ps to 500 ps.

A carrier recombination rate $R_s$ was also included at the nanowire sidewalls using the Slotboom formalism and assuming midgap surface traps as described previously[11,12]

$$R_s = \frac{2Sn_i(uv - 1)}{ue^{q\psi/kT} + ve^{-q\psi/kT} + 2}, \tag{7}$$

where $S$ is the SRV assumed equal for electrons and holes. Determination of the appropriate $S$ value will be described later.

The nanowire devices were comprised of an electrode at the bottom of the substrate and a second electrode at the top of the nanowires. The top electrode on the nanowire was treated in the model as a Schottky contact by pinning the

Fermi level at midgap. Current-voltage (I-V) curves for the single nanowire were calculated by integrating the net charge leaving the electrode at the bottom of the substrate with an applied bias. Positive bias means positive voltage applied to the top of the nanowire (i.e., forward bias (fb)) consistent with the I-V measurements. The measured current density (A $cm^{-2}$) is defined as the measured current divided by the contact area; i.e., it is the average current over the contact area, not the current density in an individual nanowire. Therefore, the single nanowire model I-V curve was multiplied by the surface density of nanowires as measured by SEM to obtain model J-V curves for comparison with the measurements. At large voltages ($V > 1$ V), the measured J-V characteristics were limited in practice by a parasitic series resistance of 3 Ω due to the measurement apparatus, which was added to the model in series with the nanowire array.

## RESULTS AND DISCUSSION

### Current-voltage measurements and model results

Model J-V characteristics, superimposed on the measured data, are shown in the log-log plots of Figure 3. Figure 3(a) shows the measured J-V characteristics for both fb (circles) and reverse bias (rb, crosses) from passivated and unpassivated nanowires. The J-V characteristics are expected to be ohmic and symmetric with respect to positive and negative bias (i.e., the nanowire should act as a simple resistor).

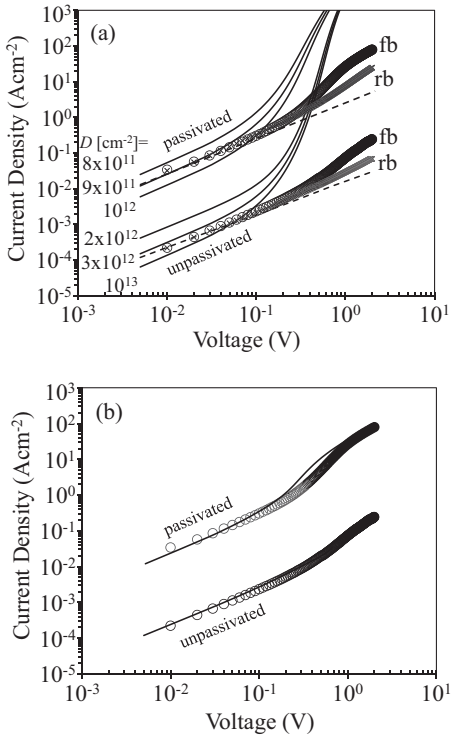


FIG. 3. Model J-V characteristics (thin solid lines for forward bias, thin dashed lines for reverse bias) superimposed on the measured data (fb = forward bias, circles; rb = reverse bias, crosses) for unpassivated and passivated nanowires. (a) Dependence of forward bias model (thin solid lines) on surface trap density $D$ without bulk or surface recombination ($\tau = \infty$, $S = 0$). (b) Forward bias J-V model (thin solid lines) using $D = 3 \times 10^{12}$ $cm^{-2}$ and $S = 1.8 \times 10^4$ cm $s^{-1}$ for unpassivated nanowires, and $D = 9 \times 10^{11}$ $cm^{-2}$ and $S = 5400$ cm $s^{-1}$ for passivated nanowires.

At low bias ($V < \sim 0.1$ V), the measured forward and reverse bias characteristics were indeed symmetric and ohmic (slope = 1 in the log-log plot) for both the passivated and unpassivated nanowires. However, at high bias ($V > \sim 1$ V), the measured forward bias characteristics showed almost an order of magnitude larger current compared to that at reverse bias. Hence, the J-V characteristics showed rectifying or diode behavior. Most importantly, the measured current for the passivated nanowires was always about two orders of magnitude larger compared to the unpassivated nanowires.

At low applied bias ($V < \sim 0.1$ V), the model J-V characteristics in Figure 3(a) were ohmic (slope = 1 in the log-log plot) under both forward bias (thin solid lines) and reverse bias (thin dashed lines) in excellent agreement with the measured data. The model resistance near zero bias was only sensitive to the surface trap density $D$. Hence, a fit of the model to the measured data at low bias can be used to estimate $D$. Three model J-V curves are indicated in Figure 3(a) for the unpassivated nanowires (lower set of curves) using different surface trap densities $D$ between $2 \times 10^{12}$ $cm^{-2}$ and $10^{13}$ $cm^{-2}$, which bounded the measured data at low applied bias. Excellent agreement is obtained between the model and the measured J-V curve for the unpassivated nanowires in the low bias regime using $D = 3 \times 10^{12}$ $cm^{-2}$, which is a typical trap density for unpassivated GaAs.[4,13]

The current density for the passivated nanowires, as shown in the upper set of curves in Figure 3(a), was approximately two orders of magnitude larger compared to the unpassivated nanowires. Within the present model, the increase in current upon passivation can only be explained by a decrease of the surface trap density $D$. In this case, $D$ refers to the trap density at the GaAs/AlInP interface. The model provided a good fit to the measured J-V characteristic of the passivated nanowires at low bias using $D$ between $8 \times 10^{11}$ $cm^{-2}$ and $10^{12}$ $cm^{-2}$, with the best fit obtained using $D = 9 \times 10^{11}$ $cm^{-2}$. This value of $D = 9 \times 10^{11}$ $cm^{-2}$ for the passivated GaAs/AlInP interface is lower than that determined earlier for the unpassivated GaAs nanowire surface where $D$ was $3 \times 10^{12}$ $cm^{-2}$. Therefore, the increase in current upon passivation can be explained by a reduction in the trap density by a factor of ~3.

The electron density $n$ and hole density $p$ obtained from the model under forward bias are plotted versus radial position in Figure 4 for the unpassivated nanowires, using the surface trap density obtained above ($D = 3 \times 10^{12}$ $cm^{-2}$). Several important observations can be made from Figure 4. The electron density $n$ is below the donor doping level of the nanowire ($10^{18}$ $cm^{-3}$) and hole accumulation occurs near the sidewalls of the nanowire. At low forward bias, the unpassivated nanowire is essentially completely depleted of charge carriers. At the surface of the nanowire near $V = 0$ V, $n$ and $p$ are approximately equal to the intrinsic carrier concentration ($n_i = 2 \times 10^6$ $cm^{-3}$), due to the Fermi level pinning near midgap from the surface traps. Note from Figure 4 that $n > p$ throughout the nanowire for each applied bias. It follows from Eqs. (3)–(5) that a net negative charge exists on the nanowire sidewalls for all biases, which is consistent with the electron depletion and hole accumulation in the nanowire. Another important observation from Figure 4 is

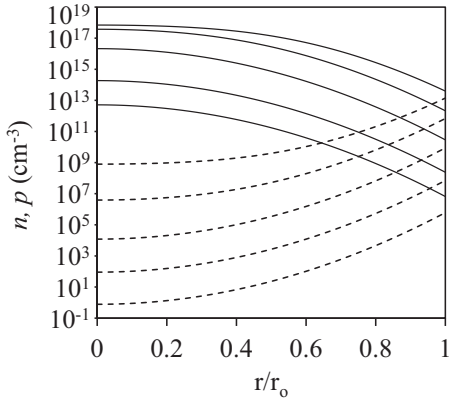


FIG. 4. Electron concentration $n$ (solid lines) and hole concentration $p$ (dashed lines) versus radial position r across an unpassivated nanowire for applied forward bias of 0, 0.25, 0.50, 0.75, and 1 V (bottom to top). The radial cross-section was taken at the mid-point along the nanowire length. $r_o$ is the nanowire radius of 26 nm.

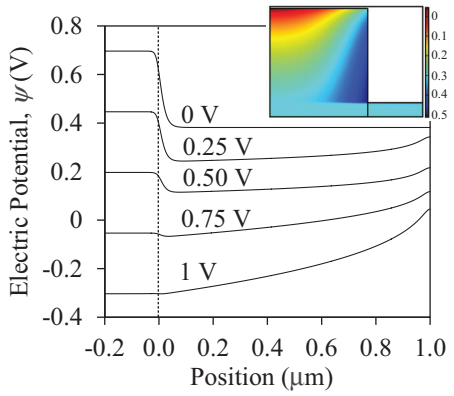


FIG. 5. Electric potential $\psi$ along the axis of an unpassivated nanowire for forward bias of 0, 0.25, 0.50, 0.75, and 1 V. The vertical dashed line located at 0 $\mu$m indicates the presence of a potential barrier at the interface between the base of the nanowire on the right and the underlying substrate on the left. The nanowire top is located at position 1 $\mu$m. Inset: the electric potential distribution in the nanowire at a forward bias of 1 V (color scale is in volts). The horizontal scale is along the nanowire radius (=26 nm) and the vertical scale is along the nanowire axis (length = 1 $\mu$m). The horizontal and vertical scales are not equal.

the occurrence of high-level injection with applied bias; i.e., $\Delta n \gg n_o$, $\Delta p \gg p_o$, where $n_o$ and $p_o$ are the carrier concentrations at zero bias. The electron density $n$ at low bias for the passivated nanowires (not shown) was two orders of magnitude higher (and $p$ was correspondingly two orders of magnitude lower) compared to the unpassivated nanowires, consistent with the higher current in the passivated nanowires.

At high forward bias ($V > \sim 0.1$ V), the simulated forward bias characteristic diverged significantly from the simulated reverse bias characteristic in Figure 3(a). Hence, the model J-V curves exhibited diode behavior in qualitative agreement with the measured data. The increase in model current at high forward bias can be attributed to two effects. First, an electrostatic potential barrier is present at the base of the nanowire where the carrier concentrations change dramatically from the space-charge region in the nanowire (see Figure 4) to the substrate (where $n = 5 \times 10^{18}$ cm$^{-3}$). Figure 5 shows the resulting electrostatic potential $\psi$ along the axis of the unpassivated nanowire for various forward biases. The potential barrier at the nanowire/substrate interface is seen to decrease under forward bias, similar to the behavior of a diode. Second, as described by Eqs. (3)–(5), the filled surface trap densities ($D_d^+$ and $D_a^-$) are dependent on $\psi$, which in turn are dependent on applied bias. The simulation results indicated that, at large forward bias, the net surface charge density decreased, simultaneous with the reduction of the nanowire/substrate potential barrier. Consequently, the nanowire resistance at high forward bias decreased greatly and approached that of an undepleted nanowire with carrier concentration $n = N_d = 10^{18}$ cm$^{-3}$ (see Figure 4).

The large discrepancy between the measured and simulated J-V curves at large forward bias in Figure 3(a) can be attributed to electron-hole recombination processes, which are excluded from the model curves of Figure 3(a). Carrier recombination is important due to the high level injection conditions in the space-charge region of the nanowire. The surface recombination velocity was determined from[4,14]

$$S = v_{th}\sigma D, \tag{8}$$

where $v_{th} = 6 \times 10^6$ cm s$^{-1}$ is the carrier thermal velocity, $\sigma \sim 10^{-15}$ cm$^2$ is the capture cross section, and $D = 3 \times 10^{12}$ cm$^{-2}$ or $9 \times 10^{11}$ cm$^{-2}$ for the unpassivated and passivated nanowires, respectively, as determined earlier. Equation (8) yields $S = 1.8 \times 10^4$ cm s$^{-1}$ and 5400 cm s$^{-1}$ for the unpassivated and passivated nanowires, respectively. The latter values of $S$ are consistent with prior work.[4,15,16] Using these $S$ values, Figure 3(b) displays the model J-V curves that includes the surface recombination, Eq. (7). It can be seen that the inclusion of surface recombination suppresses the forward bias current as compared to that in Figure 3(a), yielding an excellent fit with the measured data over the entire forward bias voltage range for both the unpassivated and passivated nanowires. The inclusion of bulk recombination, Eq. (6), in addition to the surface recombination, did not have a significant impact on the J-V curves in Figure 3(b). Therefore, the current was dominated by surface recombination even for the passivated nanowires.

Note that the forward bias current for the passivated and unpassivated nanowires exhibited a nearly quadratic behavior with bias ($I \propto V^2$) above ~0.1 V; i.e., the slope changed from 1 to 2 with increasing bias in the log-log plots of Figure 3. This behavior is often interpreted as space-charge limited current.[17–22] However, in the present model, this behavior is well explained by high level injection including recombination processes that suppress the forward bias current at large bias.

## PL measurements and model results

PL measurements were performed to further assess the change in surface trap density and surface recombination velocity upon passivation. The near band-edge PL spectra in Figure 6 showed approximately 14 times greater peak PL intensity from the passivated as compared to the unpassivated nanowires. To model the peak PL intensity from the nanowires, a carrier generation term was added to the continuity

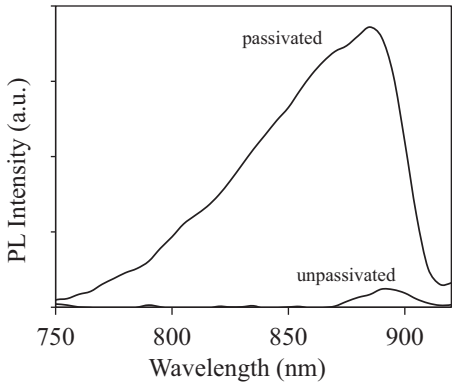


FIG. 6. Photoluminescence spectra from unpassivated and passivated nanowires.

equation, corresponding to the laser excitation. The relative peak PL intensity was obtained from the band-to-band recombination rate $R_b$

$$R_b \sim np = n_i^2 uv. \tag{9}$$

We used $D = 3 \times 10^{12}$ cm$^{-2}$ and $S = 1.8 \times 10^4$ cm s$^{-1}$ for the unpassivated nanowires, and $D = 9 \times 10^{11}$ cm$^{-2}$ and $S = 5400$ cm s$^{-1}$ for the passivated nanowires, as determined earlier. These surface parameters yielded a calculated improvement in peak PL intensity by a factor of 12 upon passivation, which is close to the experimental result of 14.

## CONCLUSIONS

AlInP shells were used to passivate the surfaces of GaAs nanowires, thereby improving their electrical transport and luminescence properties. By fitting a high injection current model to the measured J-V characteristics, including surface recombination, we determined that a reduction in surface trap density and surface recombination velocity by a factor of ~3 occurred upon passivation. Carrier depletion in the nanowire due to surface traps explained the diode behavior in the J-V curves. A fit of the simulated J-V curves to the measured data in the low bias regime yielded the surface trap density. The surface trap density was used to estimate the surface recombination velocity, which yielded an excellent fit to the high bias regime of the measured J-V curves. The resulting surface trap density and surface recombination velocity, obtained from the J-V analysis, also explained the improvement in photoluminescence upon passivation.

## ACKNOWLEDGMENTS

Financial assistance from the Natural Sciences and Engineering Research Council of Canada, Secretaría de Ciencia y Técnica de la Universidad Nacional de Tucumán (CIUNT 26/E419 and 26/E439) and FONCyT (Argentina) are gratefully acknowledged. Assistance with the TEM by Fred Pearson and with the MBE growths by Shahram Tavakoli is gratefully acknowledged.

[1]V. G. Dubrovskii, G. E. Cirlin, and V. M. Ustinov, Semiconductors **43**, 1539 (2009).
[2]M. C. Plante and R. R. LaPierre, J. Appl. Phys. **105**, 114304 (2009).
[3]B. S. Simpkins, M. A. Mastro, C. R. Eddy, Jr., and P. E. Pehrsson, J. Appl. Phys. **103**, 104313 (2008).
[4]O. Demichel, M. Heiss, J. Bleuse, H. Mariette, and A. Fontcuberta i Morral, Appl. Phys. Lett. **97**, 201907 (2010).
[5]P. Parkinson, H. J. Joyce, Q. Gao, H. H. Tan, X. Zhang, J. Zou, C. Jagadish, L. M. Herz, and M. B. Johnston, Nano Lett. **9**, 3349 (2009).
[6]I. Vurgaftmana, J. R. Meyer, and L. R. Ram-Mohan, J. Appl. Phys. **89**, 5815 (2001).
[7]A. Luque and S. Hegedus, *Handbook of Photovoltaic Science and Engineering* (Wiley, 2003).
[8]Y. Gu, Y. G. Zhang, A. Z. Li, and H. Li, Mater. Sci. Eng., B **139**, 246 (2007).
[9]A. C. E. Chia and R. R. LaPierre, Nanotechnology **22**, 245304 (2011).
[10]C. Hilsum, Electron. Lett. **10**, 259 (1974).
[11]R. R. LaPierre, J. Appl. Phys. **109**, 034311 (2011).
[12]P. E. Dodd, T. B. Stellwag, M. R. Melloch, and M. S. Lundstrom, IEEE Trans. Electron Devices **38**, 1253 (1991).
[13]A. Belghachi, Microelectron. J. **36**, 115 (2005).
[14]S. M. Sze and K. K. Ng, *Physics of Semiconductor Devices* (Wiley, 2007).
[15]L. W. Tu, E. F. Schubert, M. Hong, and G. J. Zydzik, J. Appl. Phys. **80**, 6448 (1996).
[16]E. A. Miller and G. L. Richmond, J. Phys. Chem. B **101**, 2669 (1997).
[17]K. Haraguchi, K. Hiruma, T. Katsuyama, and T. Shimada, Curr. Appl. Phys. **6**, 10 (2006).
[18]A. D. Schricker, F. M. Davidson III, R. J. Wiacek, and B. A. Korgel, Nanotechnology **17**, 2681 (2006).
[19]A. A. Talin, F. Leonard, B. S. Swartzentruber, X. Wang, and S. D. Hersee, Phys. Rev. Lett. **101**, 076802 (2008).
[20]Y. Gu and L. J. Lauhon, Appl. Phys. Lett. **89**, 143102 (2006).
[21]A. A. Talin, F. Leonard, A. M. Katzenmeyer, B. S. Swartzentruber, S. T. Picraux, M. E. Toimil-Molares, J. G. Cederberg, X. Wang, S. D. Hersee, and A. Rishinaramangalum, Semicond. Sci. Technol. **25**, 024015 (2010).
[22]A. A. Talin, B. S. Swartzentruber, F. Leonard, X. Wang, and S. D. Hersee, J. Vac. Sci. Technol. B **27**, 2040 (2009).